Fuel Gas Storage and Separations by Metal−Organic Frameworks: Simulated Adsorption Isotherms for H2 and CH4 and Their Equimolar Mixture

ARTICLE *in* THE JOURNAL OF PHYSICAL CHEMISTRY C · APRIL 2009

Impact Factor: 4.77 · DOI: 10.1021/jp809539w

2 AUTHORS, INCLUDING:

Daniel Glossman-Mitnik
Centro de Investigación en Materiales Ava…

42 PUBLICATIONS **256** CITATIONS

SEE PROFILE

Article

Fuel Gas Storage and Separations by Metal#Organic Frameworks: Simulated Adsorption Isotherms for H and CH and Their Equimolar Mixture

Marco Gallo, and Daniel Glossman-Mitnik

J. Phys. Chem. C, **2009**, 113 (16), 6634-6642• Publication Date (Web): 30 March 2009

Fuel Gas Storage and Separations by Metal−Organic Frameworks: Simulated Adsorption Isotherms for H_2 and CH_4 and Their Equimolar Mixture

Marco Gallo*,†,‡ and Daniel Glossman-Mitnik†

Grupo NANOCOSMOS and PRINATEC, Centro de Investigación en Materiales Avanzados, S.C., Miguel de Cervantes 120, Complejo Industrial Chihuahua, Chihuahua 31109, México, and Facultad de Ciencias Químicas, Universidad Autónoma de Coahuila, Boulevard Venustiano Carranza s/n, Saltillo, Coahuila 25280, México

Received: July 9, 2008; Revised Manuscript Received: March 6, 2009

Metal−organic frameworks (MOFs) are novel microporous materials with large surface areas, porosities, and thermal stabilities. Even though many thousand MOFs have been identified, few MOF materials have been evaluated for gas mixtures separations and fuel gas storage. In this work, using grand canonical Monte Carlo simulations, we calculated adsorption isotherms of pure and binary mixtures of hydrogen−methane in two large surface area MOFs (MOF-5 and MOF-177), two catenated MOFs (IRMOF-11 and MOF-14), and a high affinity open metal site MOF with strong $Zn^{\delta+}-O^{\delta-}$ dipoles on the surface that create strong energetic interaction with the adsorbates (MOF-74). The pure and mixture adsorption isotherms were calculated at 298 K and up to pressures of approximately 80 bar. The results of this study indicate that separation of hydrogen from methane in these materials would be successful, since hydrogen in a 50% bulk mixture at low pressures has selectivities on the order of 25 for MOF-74, 20 for IRMOF-11, and 18 for MOF-14, compared to low selectivities values on the order of 5 for the two large surface area MOFs, MOF-5 and MOF-177. From this study, we also found that MOF-74 has a large methane storage capacity of 170 cm^3 (STP)/cm^3 at 298 K and 35 atm, close to the 180 cm^3 (STP)/cm^3 DOE target for practical methane storage. None of the materials studied has hydrogen gravimetric uptakes in excess of 0.4% wt.

1. Introduction

Metal−organic frameworks (MOFs) are novel microporous materials with applications in the area of catalysis, adsorption separations, and gas storage.[1] They are composed of inorganic clusters bridged by organic linkers, resulting in robust solids with thermal stability. Their synthesis through reticular design allows the tailoring of materials with different porosities and functional groups. MOFs display molecular mobilities for gases that are two to three orders of magnitude higher than zeolites and active carbons.[2,3] This fast molecular transport, coupled to the absence of blocked bulk volume and the absence of significant hysteresis in their gas adsorption isotherms,[4] would make MOFs excellent materials as molecular sieves.[3] The preparation of MOFs has a further advantage in that it does not require large capital investments in synthesis technologies. In addition, the shaping of MOFs into pellets, tablets, and different geometries is not an obstacle.[3] However, despite the numerous possible advantages of MOFs in the area of adsorption separations, gas storage, and catalysis, only a few structures of the thousand available have been tested experimentally for gas separations.[5,6]

In order to enhance gas adsorption capacities, catenation of MOFs, a strategy adopted for the reduction of pore dimension, has been proposed, named framework catenation.[7] By simply distorting the primitive cubic net, by shearing along the face or body diagonals, the pores become elliptical and their shortest dimension is reduced, and the cubic net is transformed into a rhombohedral net.[7] Framework catenation can adopt the form of interpenetration, where the frameworks either are maximally displaced from each other or are interweaving where they are minimally displaced.[7−10] The reduction of the pore dimensions allows larger adsorption energies of the adsorbates with the adsorbent walls. The best adsorbents for gas storage possess a large accessible surface area, high free volume, low framework density, and a large heat of adsorption.[11,12] Catenation is believed to enhance the molecular sieve capacity of MOFs.

Hydrogen and methane have been proposed as alternative environmental friendly fuels for vehicle applications. At the present time, the majority of hydrogen production is obtained from methane steam reforming ($CH_4 + 2H_2O \rightarrow 4H_2 + CO_2$) and methane dry reforming ($CH_4 + CO_2 \rightarrow 2CO + 2H_2$).[13] The hydrogen has to be separated from methane, carbon dioxide, and smaller amounts of other gases before it can be used effectively in a fuel cell.[14] Current hydrogen separation membranes are made of palladium alloys or chemically and mechanically unstable organic polymer membranes.[15] Palladium membranes are costly and in limited supply.[15]

Separations of equimolar mixtures of hydrogen and methane by grand canonical Monte Carlo simulations have been done by Yang et al.,[5] who obtained CH_4/H_2 selectivities on the order of 20 at low pressures for a Cu-BTC MOF, and on the order of 5 for MOF-5. Similarly Liu et al.[16] studied the effect of MOFs interpenetration (catenation) on CH_4/H_2 mixture in MOFs using molecular simulation techniques. They found high CH_4/H_2 selectivities on the order of 35 for equimolar mixtures of these compounds in the catenated IRMOF-11 at pressures below 1 bar, compared to CH_4/H_2 selectivities on the order of 5 in the noncatenated IRMOF-10, IRMOF-12, and IRMOF-14. Their results showed that the adsorption selectivity of mixtures was

* Author to whom correspondence should be addressed. Phone: (52) 614-4394852. Fax: (52) 614 4394852. E-mail: marco.gallo@cimav.edu.mx.
† Centro de Investigación en Materiales Avanzados.
‡ Universidad Autónoma de Coahuila.

10.1021/jp809539w CCC: $40.75
Published on Web 03/30/2009

enhanced compared with the noninterpenetrated counterparts. A good review of molecular simulations on MOFs as well as experimental calculations (gas storage and separations) can be found on Garberoglio et al.,[17] Snurr et al.,[11] and Jiang et al.[18]

Mueller et al.[3] showed the potential of MOFs for industrial applications by testing the catalytic activation of alkynes on MOF-2, the gas purification of natural gas from tetrahydrothiophene on Cu-BTC MOF, the gas separation of a krypton−xenon mixtures on Cu-BTC MOF, the hydrogen gas storage on MOF-5 and IRMOF-8 at 77 K and 40 bar, and the self-diffusivities of ethane and benzene on MOF-5. They found that MOFs are excellent materials for industrial applications in the area of catalysis, adsorption separations, and gas storage, due to their large gas mobilities (larger than zeolites), small mass transfer resistance, and large thermal stabilities.

Mitchell et al.[19,20] have studied hydrogen−methane separations in zeolite NaA, $Na_3Zn(PO_4)_3$, zorite, ETS-4, and ETS-10 molecular sieves using molecular dynamics simulations and calculated pure adsorption isotherms by GCMC simulations. Their results showed that zeolite NaA and ETS-10 could be used for kinetic separations, but that zinc phosphate, zorite, and ETS-4 would act as true molecular sieves, allowing the separation of hydrogen from a mixture with methane. Gallo et al.[21] recently calculated absolute mixture adsorption isotherms for binary mixtures of hydrogen−methane in ETS-10 and silicalite using GCMC simulations and found that the separation of hydrogen from methane or from carbon dioxide in silicalite would be successful, since hydrogen in a 50% bulk mixture does not adsorb unless the pressure is very high, on the order of 500 bar. In contrast, in ETS-10, hydrogen in a 50% bulk mixture adsorbs at a pressure near 10 bar.

In this current work, using grand canonical Monte Carlo simulations, we calculated adsorption isotherms for pure components and for binary mixtures of hydrogen−methane in (a) two large surface area MOFs (MOF-5 and MOF-177), (b) two catenated MOFs (IRMOF-11 and MOF-14), and (c) a high affinity open metal site MOF with strong $Zn^{\delta+}-O^{\delta-}$ dipoles on the surface that create strong energetic interaction with the adsorbates (MOF-74). The objective of this work is the assessment of the separation capabilities of these novel materials for hydrogen−methane mixtures as well as their hydrogen and methane storage capabilities.

Molecular simulations can provide data for conditions that are difficult to achieve experimentally, such as large pressures and temperatures. Molecular simulations provide molecular level insight into the dynamics of the adsorbents inside the MOFs, dynamical properties such as diffusion coefficients, and calculations of thermodynamic properties such as adsorption isotherms and heats of adsorption. Molecular simulations can also screen new structures before they are synthesized and guide the synthesis of new materials designed for specific gas separations.[6,11]

2. Models and Computational Method

The materials chosen for this study are among the most porous known, exhibiting apparent Langmuir surface areas ranging from 800 m^2/g to nearly 5000 m^2/g, as determined by molecular nitrogen adsorption analyses.[4,8,22−26] IRMOF-1 (also known as MOF-5) with a surface area of 2833 m^2/g is the prototypical member of a group of isoreticular MOFs composed of octahedrally connected $Zn_4O(O_2C-)_6$ inorganic clusters bridged by linear aromatic moieties.[27,28] Its cubic topology defines a bimodal distribution of micropores that are 12 and 15 Å in diameter. IRMOF-11 is another member of this group of compounds. It has a surface area of 2096 m^2/g and is composed of longer organic links and consequently adopts an interpenetrated structure.[7] The interpenetration changes the crystal symmetry from cubic to rhombohedral and reduces the pore diameters to 7 and 12 Å. MOF-74 with a surface area of 816 m^2/g is comprised of parallel $[Zn(O-)(O_2C-)]_\infty$ chains connected by benzenoid links, delimiting a hexagonal array of channels that are 10.8 Å in diameter after the removal of coordinated solvent molecules.[8,29] MOF-14 with a surface area of 1502 m^2/g is another interpenetrated material, each framework consisting of square-connected $Cu_2(H_2O)_2(O_2C-)_4$ clusters bridged by trigonal 1,3,5-*tris*(phenylene)benzene links.[22] The cubic structure contains 16.4 Å pores connected by 7.66 × 14 Å apertures. The final material, MOF-177, has a surface area estimated at 4500 m^2/g and also is assembled from the trigonal 1,3,5-*tris*(phenylene)benzene links, in this case bridging the $Zn_4O(O_2C-)_6$ clusters also found in IRMOF-1.[24] The trigonal network contains intersecting 11.8 and 10.8 Å pores that form a 3-periodic array of channels. Further details of the structures and properties of these materials can be found in the references cited.

Models of the MOF crystal structures were adapted from the atomic coordinates reported for each material and constructed using Material Studio 4.1[30] as shown in Figure 1. Simulation cells of similar volumes were employed in the analyses of all the materials studied (as summarized in Table 1 and depicted in Figure 1). The framework atom positions were fixed during the simulations, and periodic boundary conditions were applied. Lennard-Jones (LJ) potentials were used for adsorbate−adsorbate and adsorbate−framework interactions, as commonly employed in the literature.[1,17,18] The Lorenz-Berthelot mixing rules were applied to obtain the LJ cross potentials.[31] The cutoff radii were chosen as one-half of the smallest dimension of each simulation field. The universal force field (UFF)[32] was adopted to model the framework atoms, while the Lennard-Jones parameters for H_2 ($\sigma_i = 2.915$ Å, $\epsilon_i = 0.3159$ kJ/mol) and CH_4 ($\sigma_i = 3.822$ Å, $\epsilon_i = 1.139$ kJ/mol) were used as previously.[19−21] The gases were modeled as spherical molecules (united-atom models), and quadrupolar interactions were omitted. The largest magnitude diagonalized component of the experimental quadrupole moment tensor Q_{zz} for the hydrogen molecule corresponds to 0.52 D-Å,[33] and for carbon dioxide the experimental value is −4.28 D-Å.[33] The CO_2 quadrupole moment is 8 times higher than the molecular hydrogen quadrupole moment and 100 times higher than the methane quadrupole moment. We have calculated computationally (not shown in this work) the adsorption of dioxide carbon in MOFs (MOF-5, IRMOF-11, and MOF-505) using a model for carbon dioxide that does not take into account electrostatics, and our highest error is 25% compared to the experimental results of Millward et al.[34] Since the quadrupole moment for the hydrogen molecule is eight times lower than carbon dioxide and it is the only source of contribution to the electrostatic energy, we do not expect that our error exceeds 5% by neglecting the electrostatic contribution from the molecular hydrogen quadrupole moment.

Garberoglio et al.[17] tested different models for hydrogen adsorption in metal−organic frameworks, and they found that a classical united-atom model without quadrupole interactions and without framework electrostatic interactions was in good agreement with experimental results at 298 K and pressures up to 50 bar, and at high pressures the error was less than 3−5%. A united-atom model for hydrogen adsorption without quadrupole interactions in metal−organic frameworks has been used by Snurr et al.[1] who calculated hydrogen adsorption in IRMOF-1 and IRMOF-8 and obtain reasonable agreement with experimental data. Yang et al.[5] also used a simple Lennard-Jones core

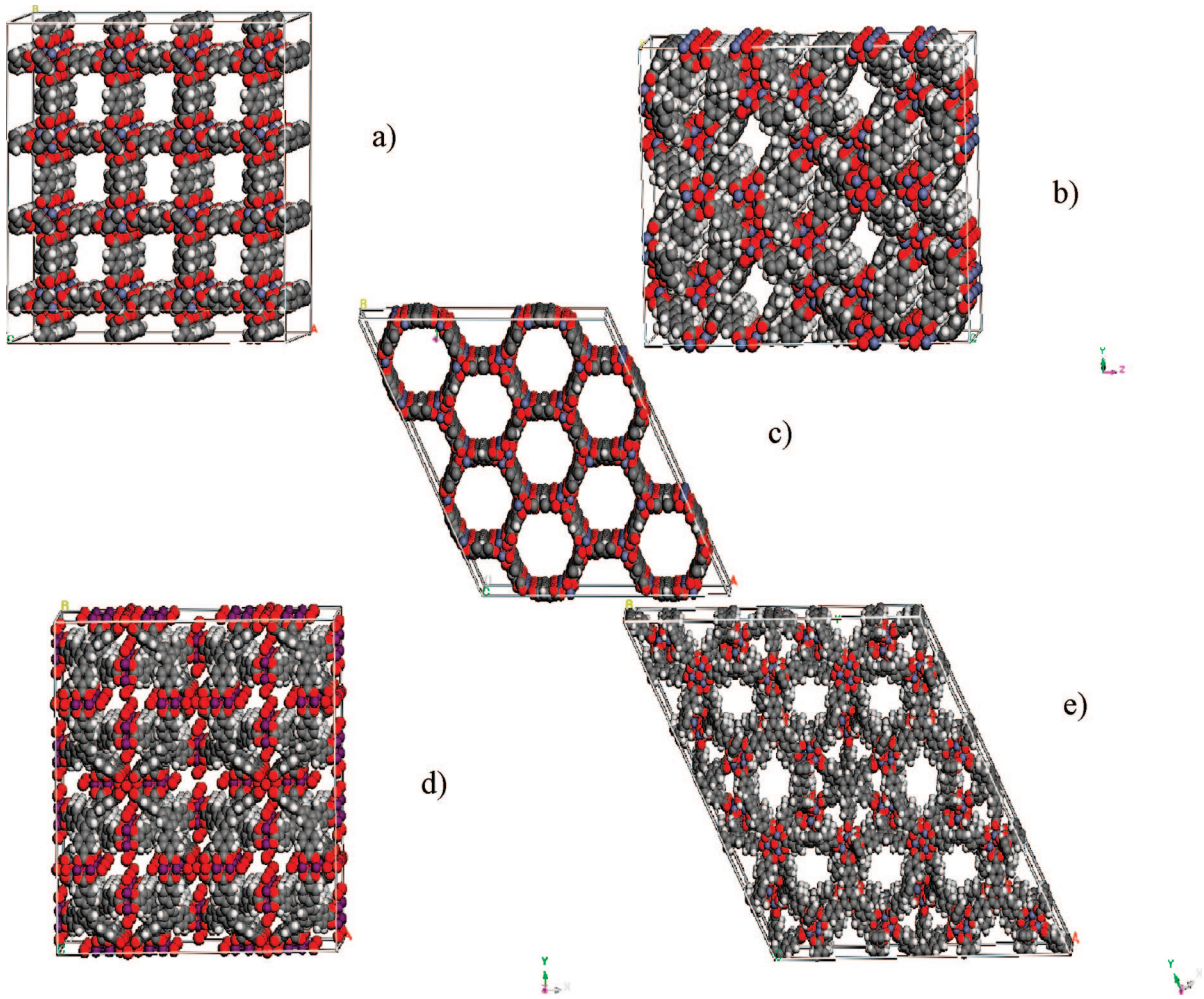

Figure 1. Space-filling representations of the materials studied in this work: (a) IRMOF-1, (b) IRMOF-11, (c) MOF-74, (d) MOF-14, and (e) MOF-177. Framework atoms are drawn as spheres: C (gray), H (white), O (red), Cu (dark purple), Zn (blue).

TABLE 1: Structural Properties of the Materials Examined

material	unit cell stoichiometry	crystal density (g/cm3)	V_p (cm^3/cm^3)	simulation field dimensions
IRMOF-1	$C_{192}H_{96}O_{104}Zn_{32}$	0.596	0.7805	$2a \times 2b \times 2c$
IRMOF-11	$C_{648}H_{432}O_{156}Zn_{48}$	0.760	0.633	$3a \times 2b \times c$
MOF-74	$C_{72}H_{18}O_{54}Zn_{18}$	1.30	0.610	$2a \times 2b \times 12c$
MOF-14	$C_{432}H_{288}Cu_{24}O_{120}$	0.757	0.605	$2a \times 2b \times 2c$
MOF-177	$C_{432}H_{240}O_{104}Zn_{32}$	0.413	0.809	$2a \times 2b \times 2c$

for hydrogen and methane, to model hydrogen and methane adsorption in two metal−organic frameworks, MOF-5 and Cu-BTC, and they found excellent agreement with experimental data. The appropriateness of these modeling approximations has also been discussed previously.[21]

2.1. One Grand Canonical Monte Carlo Simulations. In GCMC simulations the chemical potential μ_i of the fluid in the pores is kept at the same value as in the bulk phase at constant temperature and volume. The condition for fluid phase equilibrium establishes that the chemical potentials in the gas phase and adsorbate phase must be equal, allowing one to obtain the bulk pressure that corresponds to this chemical potential using an equation of state. This methodology is repeated for different chemical potentials to generate the entire adsorption isotherm.[35−38] All results presented here are for systems at room temperature, 298 K. For the pure isotherms, the configurations started with a single adsorbate randomly placed in the field and simulations were equilibrated for 3×10^6 cycles before accumulating statistics for the next 3×10^6 cycles. Each cycle consisted of a particle displacement, deletion, or insertion in the field. The average number of adsorbates in the pure isotherms averaged about 200 for hydrogen and 700 for methane. For the binary mixtures, different chemical potentials μ_i and μ_j were chosen such that the molar ratio was 1:1 in the bulk phase, as performed previously.[35] The configurations for the binary mixtures were equilibrated for 3×10^7 cycles before accumulating statistics for another 3×10^7−5×10^7 cycles. To improve the accuracy of the results, GCMC simulations for pure and mixture isotherms were divided into 10 different production periods and adsorbates averages were calculated, resulting in a standard deviation of less than 5%. Each cycle consisted of either a particle displacement, deletion, insertion, or an identity exchange in the simulation cell.[39−42] It has been reported that without introducing the identity particle exchanges, GCMC simulations of mixtures runs may not reach convergence.[43]

For the pure component isotherms, a Lennard-Jones equation of state[44] with the Gibbs−Duhem equation was used to convert

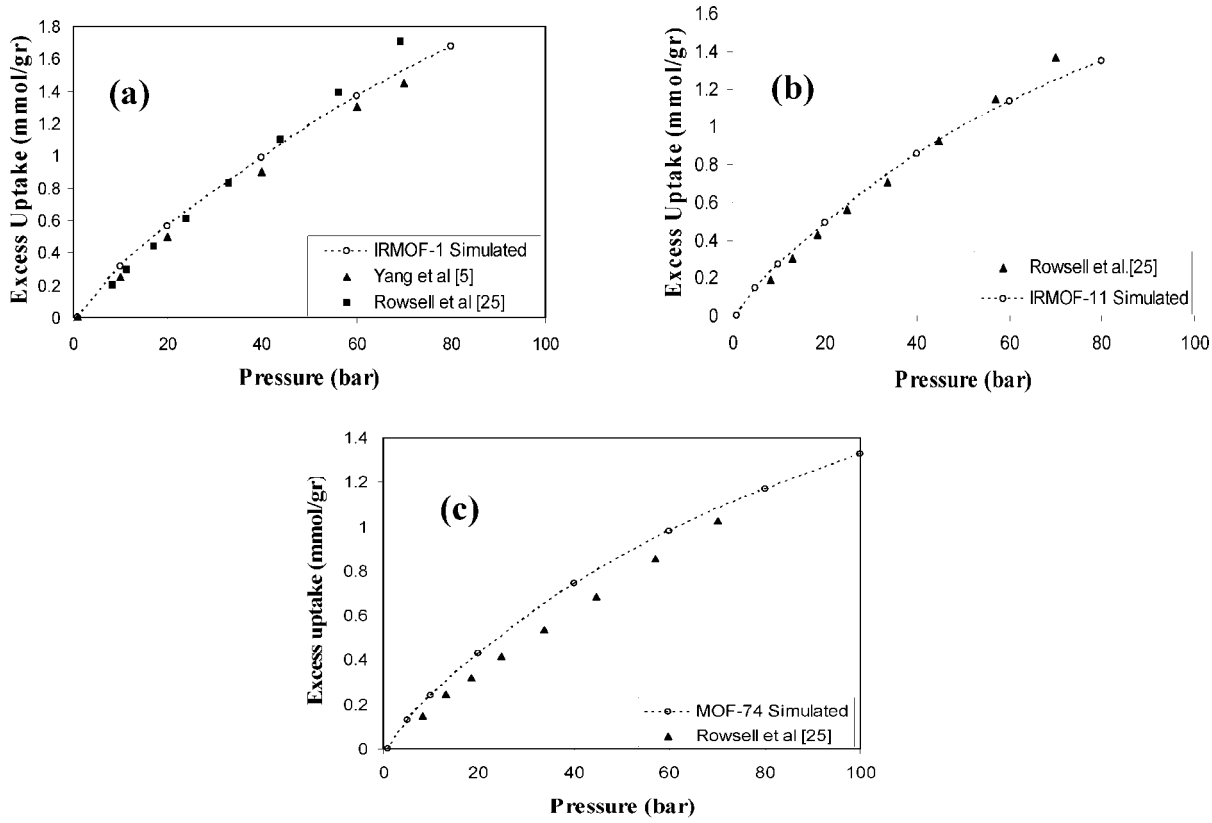

Figure 2. Comparison of simulated (open circles) and experimental room temperature excess H_2 adsorption data for (a) IRMOF-1, (b) IRMOF-11, and (c) MOF-74. References to experimental reports are provided in the legends. Trend lines have been drawn for visual aid purposes.

chemical potential units to pressure units, following the procedure of Van Tassel et al.[40,41] For the mixture isotherms, we used the following equation to calculate the chemical potentials $\hat{\mu}_i$ for each component in the mixture[45]

$$\hat{\mu}_i(T,P,x_i) = \mu_i(T,P) + RT \ln \frac{\hat{f}_i(T,P,x_i)}{f_i(T,P)} \quad (1)$$

where μ_i is the chemical potential of the pure component, R is the gas constant, T, P are the temperature and pressure, and $\hat{f}_i$, f_i are the mixture and pure fugacities. The pure and mixture fugacities were calculated using REFPROP.[46] The output of a GCMC simulation is the absolute amount adsorbed, N_{abs}, while the amount measured experimentally is the excess adsorption, N_{exc}. The excess adsorption is calculated using the following equation[6]

$$N_{exc} = N_{abs} - V_p \rho_b \quad (2)$$

where V_p is the pore volume (fluid-accessible volume) of the material and ρ_b is the bulk gas density, calculated for pure compounds using the Lennard-Jones equation of state[44] and, in the case of mixtures, using REFPROP[46] and multiplied by the component mole fraction. Pore volumes were calculated using Materials Studio 4.2[30] with a probe radius of 1.82 Å and the kinetic radius of molecular nitrogen and are tabulated in Table 1.

Validation of the simulation results was performed by comparing pure hydrogen adsorption isotherms at room temperature for IRMOF-1, IRMOF-11, and MOF-74 with previous simulations results and experimental data. As shown in Figure 2 we note good agreement between the simulated results and available H_2 adsorption data for IRMOF-1, IRMOF-11, and MOF-74.

Pure methane adsorption isotherms in IRMOF-1 were also validated against experimental data of Zhou et al.[47] and simulation results from Yang et al.[5] and Düren et al.[6] As shown in Figure 3a, we observed good agreement between our simulated results and those available from the literature.

The energetic interactions experienced by the adsorbate molecules within the adsorbent pores are related to the isosteric heat of adsorption.[12] The isosteric heat of adsorption Q_{st} is defined as[48]

$$Q_{st} = RT^2 \left[\frac{\partial \ln P}{\partial T}\right]_n \quad (3)$$

where P is the gas pressure, n is the adsorbate loading, and T is the temperature of the simulation. The isosteric heat of adsorption is obtained by differentiating a series of adsorption isotherms at different temperatures at constant loadings between 1.25 and 1.5 bar. The higher the isosteric heat of adsorption, the higher the adsorption uptake in the pores at low loadings.[8,12]

Frost et al.[1] showed the existence of three adsorption regimes for IRMOFs: at low pressures the uptake is related to the isosteric heat of adsorption, at intermediate pressures the uptakes correlates with the surface area, and at high pressure the amount adsorbed correlates with the free volume of the material.

A measure of a mixture separation is the selectivity of a porous material for different components in mixtures. The selectivity of component A relative to component B is defined as the ratio of the mole fraction of the compound of interest A in the pore x_A and bulk phases y_A over the ratio of the mole fraction of the undesired component in both the pore x_B and bulk phases y_B as defined by $S = (x_A/x_B)/(y_A/y_B)$.[49] The calculated selectivities values for the CH_4/H_2 mixtures are displayed in Figure 4.

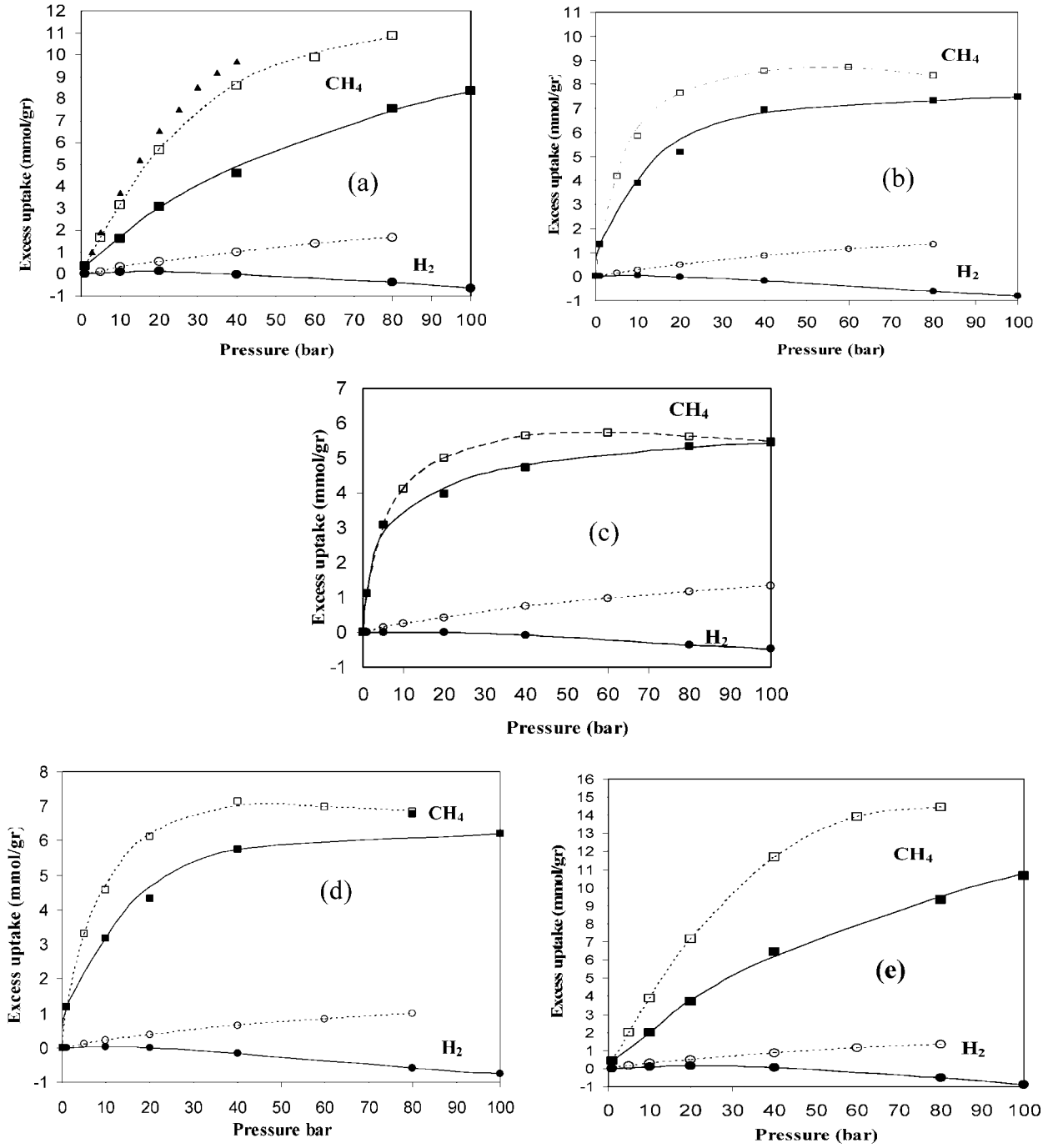

Figure 3. Excess room temperature adsorption isotherms simulated for pure CH_4 (open squares), pure H_2 (open circles), and each component of an equimolar mixture of these gases (closed symbols), in the materials (a) IRMOF-1, (b) IRMOF-11, (c) MOF-74, (d) MOF-14, and (e) MOF-177. Experimental data for methane IRMOF-1[5] are shown as filled triangles. Trend lines have been drawn for visual aid purposes.

3. Results

Table 2 displays the isosteric heat of adsorption at low loading between 1.25 and 1.5 bar for both methane and hydrogen molecules in all the structures studied. Our value of 4.65 kJ/mol for the isosteric heat of adsorption of hydrogen in MOF-5 is above the experimental value of 4.1 kJ/mol reported by Dailly et al.[50] With respect to methane, our value of 10.5 kJ/mol for the isosteric heat of adsorption in MOF-5 is in excellent agreement with the value of 10.5 kJ/mol reported by Düren et al.,[6] and with the value of 10.42 kJ/mol reported by Jiang et al.[18]

From Table 2 we can see that the isosteric heats of adsorption for hydrogen and methane are largest on MOF-74 due to strong Lennard-Jones interaction of the framework with the adsorbates. The catenated MOFs, MOF-14, and IRMOF-11 display values for the isosteric heat of adsorption that are closer in magnitude to MOF-74.

From Figure 3 it can be seen that, at low pressures up to 10 bar, both IRMOF-11 and MOF-14 possess a larger methane gravimetric uptake than MOF-5 and MOF-177, due to the larger isosteric heats of adsorption for methane on MOF-14 and IRMOF-11. At intermediate pressure, between 10 and 80 bar, MOF-5 and MOF-177 have a greater methane gravimetric uptake than their catenated counterparts. Despite a large surface area of 4500 m^2/g, MOF-177 has a volumetric capacity for methane at room temperature and 35 bar of 108 cm^3 (STP)/

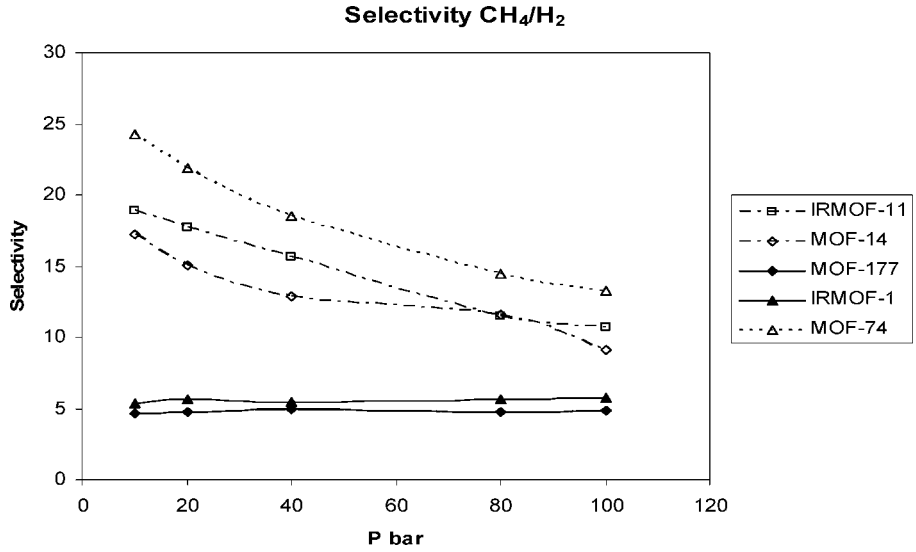

Figure 4. Selectivities values for CH_4/H_2 mixtures in MOF-5, MOF-177, IRMOF-11, MOF-14, and MOF-74 in an equimolar bulk phase.

TABLE 2: Isosteric Heats of Adsorption for Hydrogen and Methane in the Materials Examined

material	$Q_{st}(H_2)$ (kJ/mol)	$Q_{st}(CH_4)$ (kJ/mol)
IRMOF-1	4.7	10.5
IRMOF-11	6.3	18.3
MOF-74	6.5	19.1
MOF-14	6.3	18.6
MOF-177	4.4	10.2

cm^3, compared to 145 v/v for IRMOF-11 which has a surface area of 2096 m^2/g. MOF-14 has a volumetric capacity for methane of 121 v/v, and IRMOF-1 has a volumetric capacity of methane of 121 v/v. MOF-74 has the highest methane volumetric capacity of all the MOFs studied with a value of 170 v/v, close to the DOE target of 180 v/v.[12]

Garberoglio[51] using GCMC simulations recently found a new material COF-102 ("covalent organic frameworks") capable of meeting or exceeding the DOE target; the uncertainty about the correct amount of volumetric adsorption depended on whether they use the UFF (220 v/v) or the DREIDING force field (180 v/v). Based on the work of Düren et al.[12] that predicted computationally that a MOF using an anthracenedicarboxylate linker (IRMOF-993) would exceed the 180 v/v DOE target, Ma et al.[52] synthesized a new MOF called PCN-14 based on 5,5′-(9,10-anthracenediyl)diisophthalate linker capable of reaching a methane absolute adsorption of 230 v/v at 290 K and 35 bar.

From Figure 3 it is also observed that methane in the pure and mixture states has reached saturation (the adsorption isotherm starts to level off) in MOF-14, IRMOF-11, and MOF-74 at pressures around 40 bar.

None of the materials studied displays hydrogen gravimetric uptakes in excess of 0.4 wt % at room temperature and the pressures studied, in agreement with the experimental results of Rowsell et al.[25] Of all the materials studied, IRMOF-1 has the highest hydrogen gravimetric uptake of 1.67 mmol/g at 80 bar and 298 K. IRMOF-11 has a hydrogen gravimetric uptake of 1.34 mmol/g at 80 bar; MOF-177 has the same hydrogen gravimetric uptake as IRMOF-11 at 80 bar, despite having a surface area twice as large.

From Figure 4 it can be seen that the separation of hydrogen from methane in these materials would be successful, since methane in a 50% bulk mixture has a CH_4/H_2 selectivity value of 25 in MOF-74, 20 in IRMOF-11, and 17 in MOF-14, higher than the noncatenated metal organic frameworks MOF-5 and MOF-177 that possess CH_4/H_2 selectivities values on the order of 5 in agreement with the CH_4/H_2 selectivity value of 5 calculated by Yang et al.[5] in CH_4/H_2 separations in MOF-5 at equimolar bulk composition. From Figure 4 we can observe that the CH_4/H_2 selectivities values for MOF-5 and MOF-177 are nearly pressure independent, while the CH_4/H_2 selectivities values for MOF-74, IRMOF-11, and MOF-14 decrease with increasing pressure. In order to elucidate the molecular mechanism responsible for the mixture pore adsorption behavior in our materials studied in Figure 3 and responsible for our CH_4/H_2 selectivities pressure behavior, we plotted in Figure 5 the adsorbates−framework energies and adsorbate−adsorbate energies per total number of adsorbates (methane plus hydrogen) for MOF-74, IRMOF-11, and MOF-177. MOF-74 has a pore structure with well-defined pores of size 11 Å, and IRMOF-11 has different pore sizes of 7 and 11 Å and a complicated pore structure due to the catenation of the frameworks; on the other hand, MOF-177 has a large pore size of 17 Å, a large surface area, and a high pore volume.

From Figure 5 we can observe that the sorbate−sorbate energetic interactions per total number of sorbate molecules increases (becomes more attractive) with loading from 10 to 80 bar as more molecules start to occupy the pore volumes of MOFs; This sorbate−sorbate energetic increase with loading is around 0.9 times for MOF-74, 1.5 times for IRMOF-11, and 5.5 times for MOF-177. We believe that the high porosity of MOF-177 and higher adsorption saturation capacity are responsible for the higher energetic interaction increase as more sorbates are allowed to be accommodated inside the pores compared to IRMOF-11 and MOF-74 that have smaller pore sizes and thus lower porosities.

On the other hand, if we examine the sorbate−framework energetic interactions per total number of sorbate molecules with respect to loading, we observe that these interactions weaken with increasing loading as more molecules are forced on the center of the pores where the influence of the framework becomes smaller.[6] We observe that for MOF-177 the interactions with the framework decrease only about 4%, 11% for IRMOF-11, and 13% for MOF-74. Since MOF-74 has the smallest pore diameters around 11 Å and smallest surface area of all the materials studied and reaches its adsorption capacity at 40 bar, its sorbate−framework interactions start to decrease faster with respect to loading than MOF-177 as more molecule are forced

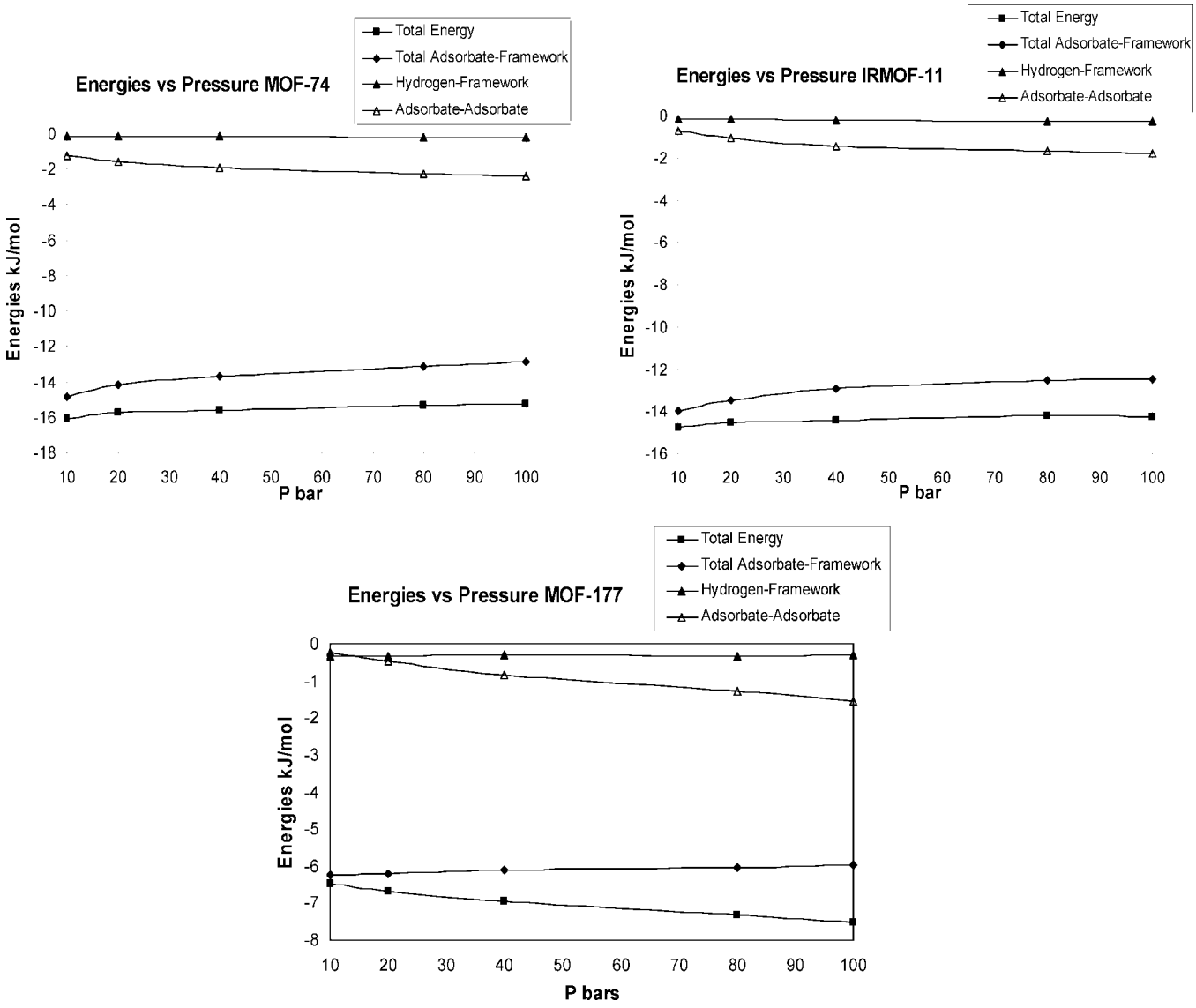

Figure 5. Sorbate−sorbate potential energies per total number of adsorbed molecules (hydrogen plus methane), sorbate−framework interaction energies per total number of adsorbed molecules, and hydrogen−framework interaction energies per total number of adsorbed molecules for MOF-74, IRMOF-11, and MOF-177.

to enter into less energetically sites, away from the influence of the framework. Because MOF-177 has six times more surface area than MOF-74 and a large pore diameter around 17 Å, and it has not reached its adsorption saturation capacity due to its high free volume at the range of pressures studied, it can accommodate more molecules near their framework atoms, and their sorbate−frameworks energetic interactions remain nearly unchanged. We believe that the constancy in the sorbate−framework energetic interactions observed in MOF-177 is responsible for its CH_4/H_2 selectivity being independent of pressure.

In Figure 5 we can observe that the strong increase in the sorbate−sorbate energetic interactions for MOF-177 with respect to loading offsets the small sorbate−framework energetic interaction decrease with respect to loading, giving rise to a decrease in total energy with respect to loading, in contrast to the increase in total energy with loading behavior observed for MOF-74 and IRMOF-11.

We plotted in Figure 6 the individual contribution of methane and hydrogen molecules to the adsorbate−framework energetic interactions with respect to loading. From this figure we observe the highest decrease in hydrogen−framework interaction is

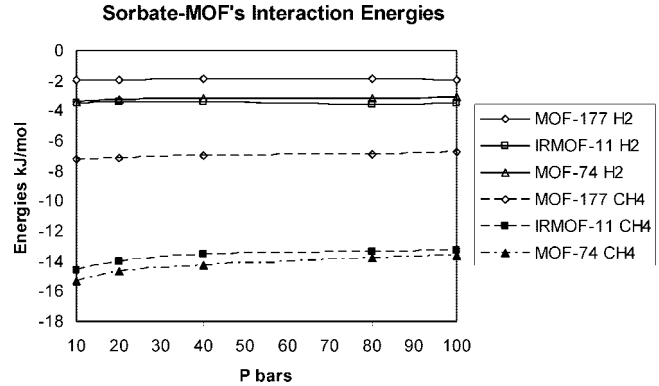

Figure 6. Methane−MOFs interaction energies and hydrogen−MOFs interaction energies versus loadings (pressures) for MOF-74, IRMOF-11, and MOF-177.

observed in MOF-74 9% compared to a decrease in hydrogen−framework interactions of less than 1% in IRMOF-11 and MOF-177. MOF-74 also has the largest decrease in methane−framework energetic interactions: 11% compared to 9% in IRMOF-11 and 5% in MOF-177.

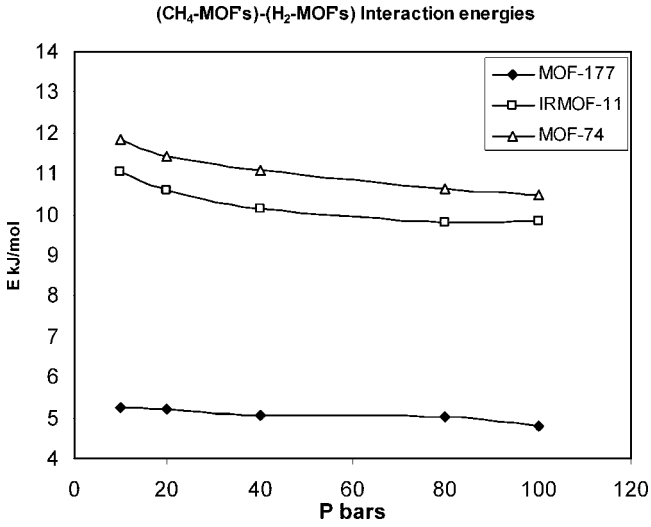

Figure 7. Absolute difference between CH_4−MOFs interaction energies and H_2−MOFs interaction energies at different loadings (pressures) for MOF-74, IRMOF-11, and MOF-177.

Recently Liu et al.,[16] by studying the effect of interprenetation (catenation) of MOFs with respect to noninterpenetrated MOFs, found that there was a decrease in the CH_4/H_2 selectivity with pressure for the catenated MOFs while in the noncatenated MOFs the CH_4/H_2 selectivity was constant. They attributed this constant selectivity in the noninterpenetrated MOFs to their simplicity in structures and large pores and the presence of a large available pore space at pressures around 20 bar. Liu et al.[16] subtracted the methane−framework energetic interaction from the hydrogen−framework energetic interactions with respect to loading and found that this difference was pressure dependent in the interpenetrated MOFs and higher than the noninterprenated MOFs resembling the same pressure dependency as their CH_4/H_2 selectivity. They found that in the noninterprenated MOFs there was only a slight decrease in the adsorbate−adsorbent interactions for both methane and hydrogen, resulting in a difference between methane and hydrogen interactions with the framework being unchanged with respect to loading, and this unchanged difference is responsible for the constant CH_4/H_2 selectivity behavior observed in their simulations.

We subtracted the methane−framework energetic interaction from the hydrogen−framework energetic interactions (interaction difference) and plotted them in Figure 7, and we observed that this difference in energetic interactions decreases with pressure for MOF-74 and IRMOF-11 as observed by Liu et al.[16] in their interprenated MOFs and in contrast to the nearly unchanged difference in interactions behavior with respect to pressure observed by Lui et al., for their noncatenated MOFs; we notice that for MOF-177 this interactions difference decreases with pressure.

The difference in methane−hydrogen framework energetic interactions is 2.2 times higher in MOF-74 than MOF-177, and 2 times higher in IRMOF-11 than MOF-177.

Keffer et al.[49] outlined the existence of a size mechanism at high pore densities where the smaller adsorbate is entropically favored, because it can pack more molecules in the pore space. Van Tassel et al.[40,41] showed competitive adsorption in Xe/Ar and Xe/CH_4 mixtures, where the smaller component and less energetic component replaces the more energetic and larger component at high pressures.

The mixture adsorption behavior observed in our simulations in Figure 3 for MOF-177 is mainly due to the energetic advantage that methane has over hydrogen as seen by the high epsilon value in the Lennard-Jones potential for methane which is 3.6 times higher than the hydrogen LJ epsilon value. Since the pore densities are not high enough to completely fill the pores in MOF-177, the entropic advantage of hydrogen over methane does not appear. This scarce entropic effect of hydrogen over methane was also showed by Yang et al.[5] in binary mixtures of hydrogen−methane in MOF-5.

The large difference in framework energetic interactions between methane and hydrogen in MOF-74 and IRMOF-11 is responsible for the high CH_4/H_2 selectivities observed in these materials with respect to MOF-177. As the pressure increases and MOF-74 and IRMOF-11 start to reach their methane adsorption saturation capacity (the adsorption isotherm starts to levels off), the energetic advantage of methane over hydrogen decreases and a small entropic advantage of hydrogen over methane appears. This pressure weakening effect of the framework energetic interactions difference of methane over hydrogen is also responsible for the pressure dependency in the CH_4/H_2 selectivities in MOF-74 and IRMOF-11.

4. Conclusions

Grand canonical Monte Carlo simulations of the equilibrium separation capabilities of four metal−organic frameworks predict that the separation of hydrogen from methane would be successful at low pressures in the catenated frameworks: MOF-14 and IRMOF-11 and in the open metal site containing MOF-74 as shown by selectivities values three times higher than the selectivities values in the noncatenated frameworks. The use of catenated frameworks and open metal site MOFs enhances the separation capabilities of MOFs at low pressures with respect to noncatenated structures and saturated metal sites MOFs as shown by CH_4/H_2 selectivities values as high as 25 at low pressures. The catenation of MOFs and the presence of coordinatively unsaturated metal sites MOFs increase the isosteric heat of adsorption, and thus the gravimetric uptake of methane at low pressures is enhanced in the catenated MOFs and open metal site MOFs. MOF-5 and MOF-177 have gravimetric capacities for methane in excess of 18 wt %, but their volumetric capacities are less than the DOE target of 180 v/v.[12] On the other hand, MOF-74 has a methane volumetric capacity of 170 v/v, which is very close to the DOE target for practical methane storage.

The large mobilities of gases in MOFs reported by Mueller et al.,[3] as well as their large hydrogen−methane separation capacities, make these novel microporous MOFs excellent materials for industrial applications in gas separations.

Acknowledgment. We are grateful to Jesse Rowsell for helpful discussions during the development of this work. M.G. gratefully acknowledges a postdoctoral fellowship from the National Science and Technology Council in Mexico (CONACyT). D.G.-M. is a CONACyT and CIMAV researcher.

References and Notes

(1) Frost, H.; Düren, T.; Snurr, R. Q. *J. Phys. Chem. B* **2006**, *110*, 9565.

(2) Stallmach, F.; Groger, S.; Kunzel, V.; Karger, J.; Yaghi, O. M.; Hesse, M.; Muller, U. *Angew. Chem., Int. Ed.* **2006**, *45*, 2123.

(3) Mueller, U.; Schubert, M.; Teich, F.; Puetter, H.; Schierle-Arndt, K.; Pastre', J. *J. Mater. Chem.* **2006**, *16*, 626.

(4) Wong-Foy, A. G.; Matzger, A. J.; Yaghi, O. M. *J. Am. Chem. Soc.* **2006**, *128*, 3494.

(5) Yang, Q.; Zhong, C. *J. Phys. Chem. B* **2006**, *110*, 17776.

(6) Düren, T.; Snurr, R. Q. *J. Phys. Chem. B* **2004**, *108*, 15703.

(7) Rowsell, J. L. C.; Yaghi, O. M. *Angew. Chem., Int. Ed.* **2005**, *44*, 4670.
(8) Rowsell, J. L. C.; Yaghi, O. M. *J. Am. Chem. Soc.* **2006**, *128*, 1304.
(9) Kesanli, B.; Cui, Y.; Smith, M. R.; Bittner, E. W.; Bockrath, B. C.; Lin, W. *Angew. Chem., Int. Ed.* **2005**, *44*, 72.
(10) Sun, D.; Ma, S.; Ke, Y.; Collins, D. J.; Zhou, H. *J. Am. Chem. Soc.* **2006**, *128*, 3896.
(11) Snurr, R. Q.; Hupp, J. T.; Nguyen, S. T. *AIChE J.* **2004**, *50*, 1090.
(12) Düren, T.; Sarkisov, L.; Yaghi, O. M.; Snurr, R. Q. *Langmuir* **2004**, *20*, 2683.
(13) Nenoff, T. M. Defect-free thin film zeolite membranes for hydrogen separation and isolation, DOE/H_2 Annual Review meeting, May 19, 2003.
(14) Thomas, S.; Zalbowitz, M.; Cruz, J. Fuel cells—green power, Los Alamos National Laboratory, 1999.
(15) Welk, M. E.; Nenoff, T. M.; Bonhomme, F. *Studies in Surfaces and Catalysis*; Elsevier B.V.: New York, 2004; Vol. 154.
(16) Liu, B.; Yang, Q.; Xue, C.; Zhong, C.; Chen, B.; Smit, B. *J. Phys. Chem. C* **2008**, *112*, 9854.
(17) Garberoglio, G.; Skoulidas, A. I.; Johnson, J. K. *J. Phys. Chem. B* **2005**, *109*, 13094.
(18) Jiang, J.; Sandler, S. I. *Langmuir* **2006**, *22*, 5702.
(19) Mitchell, M. C.; Autry, J. D.; Nenoff, T. M. *Mol. Phys.* **2001**, *99*, 1831.
(20) Mitchell, M. C.; Gallo, M.; Nenoff, T. M. *J. Chem. Phys.* **2004**, *121*, 1910.
(21) Gallo, M.; Mitchell, M. C.; Nenoff, T. M. *Fluid Phase Equilib.* **2006**, *247*, 135.
(22) Chen, B.; Eddaoudi, M.; Hyde, S. T.; O'Keeffe, M.; Yaghi, O. M. *Science* **2001**, *291*, 1021.
(23) Rowsell, J. L. C.; Millward, A. R.; Park, K. S.; Yaghi, O. M. *J. Am. Chem. Soc.* **2004**, *126*, 5666.
(24) Chae, H. K.; Siberio-Perez, D. Y.; Kim, J.; Go, Y.; Eddaoudi, M.; Matzger, A. J.; O'Keeffe, M.; Yaghi, O. M. *Nature (London)* **2004**, *427*, 523.
(25) Rowsell, J. L. C. Ph.D. Dissertation, University of Michigan, 2005.
(26) Panella, B.; Hirscher, M.; Pütter, H.; Müller, U. *Adv. Funct. Mater.* **2006**, *16*, 520.
(27) Li, H.; Eddaoudi, M.; O'Keeffe, M.; Yaghi, O. M. *Nature (London)* **1999**, *402*, 276.
(28) Eddaoudi, M.; Kim, J.; Rosi, N.; Vodak, D.; Wachter, J.; O'Keeffe, M.; Yaghi, O. M. *Science* **2002**, *295*, 469.
(29) Rosi, N. L.; Kim, J.; Eddaoudi, M.; Chen, B.; O'Keeffe, M.; Yaghi, O. M. *J. Am. Chem. Soc.* **2005**, *127*, 1504.
(30) Accelrys Inc, Material Studio, 4.2, Accelrys Inc, San Diego, CA, 2005.
(31) Bird, R.; Stewart, W.; Lightfoot, E. *Transport Phenomena*; John Wiley & Sons: New York, 2001.
(32) Rappe, A. K.; Casewit, C. J.; Colwell, K. S.; Goddard, W. A., III; Skiff, W. M. *J. Am. Chem. Soc.* **1992**, *114*, 10024.
(33) NIST: Computational Chemistry Comparison and Benchmark DataBase release 14, 2006, http://cccbdb.nist.gov/.
(34) Millward, A. R.; Yaghi, O. M. *J. Am. Chem. Soc.* **2005**, *127*, 17998.
(35) Shevade, A. V.; Jiang, S.; Gubbins, K. E. *J. Chem. Phys.* **2000**, *113*, 6933.
(36) Allen, M. P.; Tildesley, D. J. *Computer Simulation of Liquids*; Oxford University Press: Oxford, 1987.
(37) Frenkel, D.; Smit, B. *Understanding Molecular Simulations*; Academic Press: San Diego, CA, 1996.
(38) Gupta, A.; Clark, L. A.; Snurr, R. Q. *Langmuir* **2000**, *16*, 3910.
(39) Kofke, D. A. *Mol. Simul.* **1991**, *7*, 285.
(40) Van Tassel, P. R.; Davis, H. T.; McCormick, A. V. *Langmuir* **1994**, *10*, 1257.
(41) Van Tassel, P. R.; Davis, H. T.; McCormick, A. V. *Mol. Simul.* **1996**, *17*, 239.
(42) Adhangale, P.; Keffer, D. *Langmuir* **2002**, *18*, 10455.
(43) Fuchs, A. H.; Cheetham, A. K. *J. Phys. Chem. B* **2001**, *105*, 7374.
(44) Nicolas, J. J.; Gubbins, K. E.; Streett, W. B.; Tildesley, D. J. *Mol. Phys.* **1979**, *37*, 1429.
(45) Tester, J. W.; Modell, M. *Thermodynamics and Its Applications*, 3rd. ed.; Prentice-Hall: New York, 1997.
(46) NIST Reference Fluid Thermodynamic and Transport Properties Database (REFPROP), Version 7.0, National Institute of Standards and Technology, Gaithersburg, MD.
(47) Zhou, W.; Wu, H.; Hartman, M. R.; Yildrim, T. *J. Phys. Chem. C* **2007**, *111*, 16131.
(48) Hill, T. L. *J. Chem. Phys.* **1949**, *17*, 520.
(49) Keffer, D.; Davis, H. T.; McCormick, A. V. *J. Phys. Chem.* **1996**, *100*, 638.
(50) Dailly, A.; Vajo, J. J.; Ahn, C. C. *J. Phys. Chem. B* **2006**, *110*, 1099.
(51) Garberoglio, G. *Langmuir* **2007**, *23*, 12154.
(52) Ma, S.; Sun, D.; Simmons, J. M.; Collier, C. D.; Yuan, D.; Zhou, H. *J. Am. Chem. Soc.* **2008**, *130*, 1012.

JP809539W